SCIENCE CHINA
Information Sciences

• RESEARCH PAPER •

February 2019, Vol. 62 022302:1–022302:15
https://doi.org/10.1007/s11432-017-9322-2

Quantitative SNR analysis of QFM signals in the LPFT domain with Gaussian windows

Yan-Na ZHANG[1,2], Bing-Zhao LI[1,2*], Navdeep GOEL[3] & Salvador GABARDA[4]

[1]*School of Mathematics and Statistics, Beijing Institute of Technology, Beijing* 100081, *China;*
[2]*Beijing Key Laboratory on MCAACI, Beijing Institute of Technology, Beijing* 100081, *China;*
[3]*Electronics and Communication Engineering Section, Yadavindra College of Engineering, Punjabi University Guru Kashi Campus, Talwandi Sabo* 151302, *India;*
[4]*Instituto de Óptica, Spanish Council for Scientific Research* (*CSIC*), *Madrid* 28006, *Spain*

Received 7 April 2017/Revised 24 November 2017/Accepted 8 January 2018/Published online 15 October 2018

Abstract The purpose of this paper is to present a quantitative SNR analysis of quadratic frequency modulated (QFM) signals. This analysis is located in the continuous-time local polynomial Fourier transform (LPFT) domain using a Gaussian window function based on the definition of 3 dB signal-to-noise ratio (SNR). First, the maximum value of the local polynomial periodogram (LPP), and the 3 dB bandwidth in the LPFT domain for a QFM signal is derived, respectively. Then, based on these results, the 3 dB SNR of a QFM signal with Gaussian window function is given in the LPFT domain with one novel idea highlighted: the relationship among standard SNR, parameters of QFM signals and Gaussian window function is clear, and the potential application is demonstrated in the parameter estimation of a QFM signal using the LPFT. Moreover, the 3 dB SNR in the LPFT domain is compared with that in the linear canonical transform (LCT) domain. The validity of theoretical derivations is confirmed via simulation results. It is shown that, in terms of SNR, QFM signals in the LPFT domain can achieve a significantly better performance than those in the LCT domain.

Keywords SNR analysis, quadratic frequency modulated signal, local polynomial Fourier transform, linear canonical transform, time frequency representations

Citation Zhang Y-N, Li B-Z, Goel N, et al. Quantitative SNR analysis of QFM signals in the LPFT domain with Gaussian windows. Sci China Inf Sci, 2019, 62(2): 022302, https://doi.org/10.1007/s11432-017-9322-2

1 Introduction

Time frequency representations (TFRs), which provide effective information about joint time and frequency, have drawn much more attention in analyzing non-stationary signals in various areas including image processing, radar signal analysis and communication systems [1–6]. One of the most important features of these techniques is that they can concentrate signals in a relatively small region while spreading noise in the whole transformed domain. It can be explained as an increase of the regional signal-to-noise ratio (SNR) in the time-frequency (TF) domain compared with that in either the time domain or frequency domain alone [7]. Since noise widely exists in the real world, various practical areas face the problems of noise analysis [1,8]. The aforementioned feature makes TFRs to minimize the effect of noise and offer a better performance in broad practical applications, especially for signal detection by using the thresholding. Moreover, it is a key factor to evaluate the performance of different TF distributions [9]. Therefore, the quantitative SNR analysis of different TFRs has been an important issue [10, 11].

* Corresponding author (email: li_bingzhao@bit.edu.cn)

Many aspects of noise analysis regarding TFRs have been well discussed [12–14]. To be specific, extensive noise signal analysis and comparisons between the short-time Fourier transform (STFT), and Wigner-Ville distribution (WVD) have been performed well [12, 13]. The influence of noise to the STFT and bilinear distributions of Cohen's class have been presented in terms of output SNR [14]. Furthermore, other studies on the SNR analysis are regarding the maximal peaks like peak signal-to-noise ratio (PSNR) or the whole line integrations, i.e., the conventional SNR defined as a ratio of the mean power of the signal over the mean power of the noise. However, the output SNR, PSNR and conventional SNR cannot work fine for the non-stationary signals because the SNR definition should be transform-domain dependent and closely relates to the bandwidth of a signal occupied in that domain [7]. Thus, researchers begin to focus on a 3 dB SNR analysis of given signals, which is a different definition firstly proposed by Xia [7]. 3 dB SNR is quite proper in the joint TF domain under different TFRs as well as in the time domain and frequency domain alone. The quantitative SNR analyses using 3 dB SNR for the LFM signal, a valuable kind of non-stationary signals in radar [15], based on different TFRs have been well investigated, such as the STFT [7, 11], the PWVD [16], the local polynomial Fourier transform (LPFT) [10, 17] and the linear canonical transform (LCT) [18].

Besides, a quadratic frequency modulated (QFM) signal is also an important kind of non-stationary signals, which can be found in nature and engineering applications widely such as radar, sonar, speech [19, 20], and communication field, especially in radar systems. One of its most important applications is in imaging of inverse synthetic aperture radar (ISAR) for moving targets [19, 21]. When the target has a high maneuvering movement, the received signal of the target can be modeled as QFM signals [21, 22]. The cubic phase of the QFM signal provides crucial dynamic parameters of moving target in the radar systems. In the real applications, the TFRs-based method of a QFM signal is often used and performances of analysis results are strongly affected by the noise. So, it is interesting and worthwhile to investigate the SNR analysis for QFM signals associated with different TFRs to further satisfy the requirement of practical applications.

In this paper, a quantitative SNR analysis of a QFM signal in the LPFT domain with a Gaussian window function based on 3 dB SNR has been presented in detail. The rest of the paper is organized as follows. After briefly reviewing the basic definitions of the LPFT, LCT and 3 dB SNR in Section 2, the quantitative SNR analysis for QFM signals in the LPFT domain is derived by using three separate theorems in Section 3. To verify the derived results, a simulation comparison is performed on SNRs in the LPFT and the LCT domain in Section 4. As a potential application of the aforementioned results, the parameter estimation performance of QFM signal is provided in Section 5 using the LPFT and the LCT, respectively. Finally, conclusion is provided in Section 6.

2 Preliminaries

Before deriving the quantitative SNR analysis for a QFM signal, some basic notions are introduced here.

2.1 Local polynomial Fourier transform

The local polynomial Fourier transform (LPFT), as a generalization of the STFT, has been a powerful analysis tool in many different applications in recent years. The LPFT of a signal $x(t)$ with a window function $h(t)$ is defined as [17, 23]

$$\mathrm{LPFT}_x^M(t,\bar{w}) = \int_{-\infty}^{\infty} x(t+\tau)h^*(\tau)\mathrm{e}^{-\mathrm{j}\theta(\tau,\bar{w})}\mathrm{d}\tau, \tag{1}$$

where

$$\begin{aligned} \theta(\tau,\bar{w}) &= w\tau + w_1\tau^2/2 + \cdots + w_{M-1}\tau^M/M!, \\ \bar{w} &= (w, w_1, \ldots, w_{M-1}), \end{aligned} \tag{2}$$

the asterisk denotes a complex conjugate value, and M is the order of the LPFT. Here and in what follows the integral are taken over $(-\infty, \infty)$ if unspecified. The energy distribution of the LPFT, or the local polynomial periodogram (LPP), is defined as [17]

$$\mathrm{LPP}_x^M(t, \bar{w}) = |\mathrm{LPFT}_x^M(t, \bar{w})|^2. \tag{3}$$

Since the LPFT can significantly improve the resolution of the TF analysis compared with the STFT, and is free from cross terms that exist in the WVD, it has been a significant tool to deal with non-stationary signals whose frequency varies over time. Moreover, the LPFT has been widely used in ISAR imaging to improve radar images of fast maneuvering targets [10, 24], and spread spectrum communications to achieve improved performance compared with that obtained by the STFT [25]. Various other applications of the LPFT can also be found in [17].

2.2 Linear canonical transform

The linear canonical transform (LCT) is a three free parameters class of linear integral transforms, which is defined as [26, 27]

$$\mathrm{LCT}_x^A(u) = \int x(t) K_A(t, u) \mathrm{d}t, \tag{4}$$

where the kernel function is

$$K_A(t, u) = \begin{cases} \dfrac{1}{\sqrt{\mathrm{j}2\pi b}} \mathrm{e}^{\mathrm{j}(\frac{du^2}{2b} - \frac{ut}{b} + \frac{at^2}{2b})}, & b \neq 0, \\ \sqrt{d} \mathrm{e}^{\mathrm{j}\frac{cdu^2}{2}} \delta(t - du), & b = 0. \end{cases} \tag{5}$$

Herein, $A = (a, b, c, d)$ is a real parameter matrix of the LCT satisfying $ad - bc = 1$. It includes the classical Fourier transform (FT), the fractional Fourier transform (FRFT), the Fresnel transform, as well as other transforms as its special cases [27–30]. Many important theories related to the LCT such as convolution and correlation, sampling theorem and uncertainty principles have been well investigated in [31–34]. With more degrees of freedom compared with FT and FRFT, the LCT is much more flexible but with similar computation cost as the conventional FT does. It is widely applied in optics and engineering under this advantage [26, 27]. Considering the local features of non-stationary signals, the LCT is used with a window function and defined as follows [35]:

$$\mathrm{LCT}_x^A(t, u) = \int x(t + \tau) h^*(\tau) K_A(\tau, u) \mathrm{d}\tau. \tag{6}$$

Similar to that in [10], a Gaussian function as the window is used in this paper, which is defined as

$$h(\tau) = \left(\frac{\alpha}{\pi}\right)^{1/4} \mathrm{e}^{(-\frac{\alpha}{2}\tau^2)}, \quad \alpha > 0, \tag{7}$$

where α is a parameter that controls the width of the window function. For more details about the windowed LCT and its special cases, the readers can refer to [35–37].

2.3 3 dB signal-to-noise ratio

The conventional SNR is defined as the ratio of the mean power of the signal over the mean power of the noise, where the mean is taken over the whole time domain. This definition is not suitable for the non-stationary signals, especially for narrow bandwidth signals. Hence, a different definition of SNR named as 3 dB SNR is adopted in this paper, which is firstly introduced by Xia [7]. Considering a signal $x(\Omega)$ corrupted by an additive noise:

$$y(\Omega) = x(\Omega) + \eta(\Omega), \tag{8}$$

where $x(\Omega)$ is an original signal, and $\eta(\Omega)$ is additive white Gaussian noise (AWGN) with zero mean and variance σ^2. Ω is a variable which can stand for time t, frequency w, or the joint time-frequency (t, w). The 3 dB SNR is defined as [7]

$$\mathrm{SNR}^{3\ \mathrm{dB}} = \frac{\int_{\chi} |x(\Omega)|^2 \mathrm{d}\Omega}{|\chi|\sigma^2}. \tag{9}$$

Here $|\chi|$ denotes the cardinality of the set χ and is called as 3 dB bandwidth. Besides, the set χ is

$$\chi = \{\Omega : |x(\Omega)|^2 > 0.5 \max |x(\Omega)|^2\}. \tag{10}$$

Also the PSNR (defined by the ratio of the peak squared magnitude over the mean noise power) cannot be valid if signals contain more than one peak value such as the curves in the TF domain [38]. Examples shown in [7] have illustrated better indication of signal and noise levels in various domains.

3 SNR analysis for the QFM signal

In this section, a 3 dB SNR analysis of QFM signals in terms of the LPFT is provided. Different from the method in [10] based on the relationship between the LPFT and the WVD, the proposed method in this paper is mainly explored using some mathematical techniques. With the order increase of the LPFT, the 3 dB bandwidth with $M = 3$ is more complicated than that of the LPFT when $M = 2$ in [10]. Based on the maximum of the LPP derived in Theorem 1, Theorem 2 provides an approximate expression of the 3 dB bandwidth for the QFM signal in the third LPFT domain. With the aforementioned results, 3 dB SNR for a QFM signal is finally presented in Theorem 3. The specific results are as follows.

Theorem 1. The spectrum of the QFM signal $x(t) = A\mathrm{e}^{\mathrm{j}(a_0 t + \frac{a_1}{2}t^2 + \frac{a_2}{3!}t^3)}$ in the LPFT domain of order $M = 3$ reaches a constant finite maximum value for any time t and frequencies w, w_1, w_2, which is given by

$$\max_{(t,\bar{w})} \mathrm{LPP}_x^3(t, \bar{w}) = 2A^2\sqrt{\frac{\pi}{\alpha}}, \tag{11}$$

where w_2 frequency is independent of time and has value $w_2 = a_2$.

Proof. Let the order of LPFT be $M = 3$. Then the LPFT of a QFM signal can be simplified as

$$\begin{aligned}\mathrm{LPFT}_x^3(t, \bar{w}) = {} & A\left(\frac{\alpha}{\pi}\right)^{\frac{1}{4}} \mathrm{e}^{\mathrm{j}(a_0 t + \frac{a_1}{2}t^2 + \frac{a_2}{3!}t^3)} \\ & \times \int \mathrm{e}^{\mathrm{j}(a_0 + a_1 t + \frac{a_2}{2}t^2 - w)\tau + \mathrm{j}\frac{(a_1 + a_2 t - w_1)}{2}\tau^2 + \mathrm{j}\frac{(a_2 - w_2)}{3!}\tau^3} \mathrm{e}^{-\frac{\alpha}{2}\tau^2} \mathrm{d}\tau. \end{aligned} \tag{12}$$

Let

$$\varphi(\tau) = \left(a_0 + a_1 t + \frac{a_2}{2}t^2 - w\right)\tau + \frac{(a_1 + a_2 t - w_1)}{2}\tau^2 + \frac{(a_2 - w_2)}{3!}\tau^3, \tag{13}$$

where $\varphi(\tau)$ is a real function about the variable τ. The maximum of the LPP of signal $x(t)$ is obtained as follows:

$$\mathrm{LPP}_x^3(t, \bar{w}) \leqslant A^2\left(\frac{\alpha}{\pi}\right)^{\frac{1}{2}} \left(\int |\mathrm{e}^{-\frac{\alpha}{2}\tau^2} \cdot \mathrm{e}^{\mathrm{j}\varphi(\tau)}| \mathrm{d}\tau\right)^2 = 2A^2\sqrt{\frac{\pi}{\alpha}}. \tag{14}$$

The above inequality becomes an equality and it is satisfied independently of the variable τ if and only if

$$\mathrm{e}^{-\frac{\alpha}{2}\tau^2} \cdot \mathrm{e}^{\mathrm{j}\varphi(\tau)} = |\mathrm{e}^{-\frac{\alpha}{2}\tau^2} \cdot \mathrm{e}^{\mathrm{j}\varphi(\tau)}| = \mathrm{e}^{-\frac{\alpha}{2}\tau^2}, \tag{15}$$

i.e.,

$$\varphi(\tau) = 0. \tag{16}$$

According to (13), that means

$$\begin{cases} a_0 + a_1 t + \dfrac{1}{2} a_2 t^2 - w = 0, \\ \dfrac{1}{2}(a_1 + a_2 t - w_1) = 0, \\ \dfrac{1}{3!}(a_2 - w_2) = 0. \end{cases} \tag{17}$$

For any arbitrary value of the time variable, t, the frequency values that meet conditions (17) are

$$\begin{cases} w = a_0 + a_1 t + \dfrac{1}{2} a_2 t^2, \\ w_1 = a_1 + a_2 t, \\ w_2 = a_2. \end{cases} \tag{18}$$

The peak of instantaneous energy in the LPFT domain can arrive at the maximum

$$\max_{(t,\bar{w})} \mathrm{LPP}_x^3(t, \bar{w}) = 2A^2 \sqrt{\frac{\pi}{\alpha}}, \tag{19}$$

when all three conditions in (17) are satisfied. However, the main target of attention is in condition $w_2 = a_2$, because it is the only one that is independent of time and it will be greatly helpful for simplification in the derivation of the quantitative SNR analysis. Such simplification will avoid the calculation of the cubic exponential related with the $M = 3$ order in the LPFT integral, which leads to a transcendental function related to Airy function [39].

Theorem 2. The 3 dB bandwidth for the QFM signal $x(t)$ in the LPFT domain, bounded to $w_2 = a_2$, is a surface whose base contour is delimited by a line $f(w, w_1) = A^2\sqrt{\pi/\alpha}$ inscribed in a rectangular area whose limits are related to the window parameter α and the QFM phase $\varphi(t)$ by the following relationship:

$$\begin{cases} \chi_w = \{w : \dot{\varphi}(t) - \sqrt{\alpha \ln 2} \leqslant w \leqslant \dot{\varphi}(t) + \sqrt{\alpha \ln 2}\}, \\ \chi_{w_1} = \{w_1 : \ddot{\varphi}(t) - \sqrt{3}\alpha \leqslant w_1 \leqslant \ddot{\varphi}(t) + \sqrt{3}\alpha\}, \end{cases} \tag{20}$$

where $\dot{\varphi}$ and $\ddot{\varphi}$ are the time derivatives of $\varphi(t) = a_0 t + \frac{a_1}{2} t^2 + \frac{a_2}{3!} t^3$, the phase of the QFM signal.

Proof. Letting $w_2 = a_2$ in (12) and given that the function under the integral sign is continuous on the domain of application, the continuity theorem for improper integrals [40] determines that the LPFT of our interest becomes

$$\begin{aligned} \mathrm{LPFT}_x^3(t, \bar{w}) \mid_{w_2 = a_2} &= A \left(\frac{\alpha}{\pi}\right)^{\frac{1}{4}} \mathrm{e}^{\mathrm{j}(a_0 t + \frac{a_1}{2} t^2 + \frac{a_2}{3!} t^3)} \int \mathrm{e}^{[-\frac{\alpha + \mathrm{j}(w_1 - a_1 - a_2 t)}{2} \tau^2 - \mathrm{j}(w - a_0 - a_1 t - \frac{a_2}{2} t^2)\tau]} \mathrm{d}\tau \\ &= A \left(\frac{\alpha}{\pi}\right)^{\frac{1}{4}} \mathrm{e}^{\mathrm{j}(a_0 t + \frac{a_1}{2} t^2 + \frac{a_2}{3!} t^3)} \cdot \sqrt{\frac{2\pi}{\alpha + \mathrm{j}(w_1 - a_1 - a_2 t)}} \mathrm{e}^{-\frac{(w - a_0 - a_1 t - \frac{a_2}{2} t^2)^2}{2[\alpha + \mathrm{j}(w_1 - a_1 - a_2 t)]}}, \end{aligned} \tag{21}$$

and

$$\mathrm{LPP}_x^3(t, \bar{w}) \mid_{w_2 = a_2} = \frac{2A^2\sqrt{\pi} \cdot |\mathrm{e}^{-\frac{(w - a_0 - a_1 t - \frac{a_2}{2} t^2)^2}{2[\alpha + \mathrm{j}(w_1 - a_1 - a_2 t)]}}|^2}{\sqrt{\alpha + \frac{1}{\alpha}(w_1 - a_1 - a_2 t)^2}}. \tag{22}$$

Let

$$\begin{cases} m = w_1 - a_1 - a_2 t, \\ n = -\dfrac{(w - a_0 - a_1 t - \frac{a_2}{2} t^2)^2}{2}, \end{cases} \tag{23}$$

then

$$\left|\mathrm{e}^{-\frac{(w-a_0-a_1t-\frac{a_2}{2}t^2)^2}{2[\alpha+\mathrm{j}(w_1-a_1-a_2t)]}}\right|^2=\left|\mathrm{e}^{\frac{n}{\alpha+\mathrm{j}m}}\right|^2=\mathrm{e}^{-\frac{(w-a_0-a_1t-\frac{a_2}{2}t^2)^2}{\alpha+\frac{1}{\alpha}(w_1-a_1-a_2t)^2}}, \tag{24}$$

and

$$\mathrm{LPP}_x^3(t,\bar{w})\mid_{w_2=a_2}=\frac{2A^2\sqrt{\pi}\cdot\mathrm{e}^{-\frac{(w-a_0-a_1t-\frac{a_2}{2}t^2)^2}{\alpha+\frac{1}{\alpha}(w_1-a_1-a_2t)^2}}}{\sqrt{\alpha+\frac{1}{\alpha}(w_1-a_1-a_2t)^2}}. \tag{25}$$

Also, we have the following relationships for the phase $\varphi(t)$ of the QFM signal.

$$\begin{cases}\varphi(t)=a_0t+\dfrac{a_1}{2}t^2+\dfrac{a_2}{3!}t^3,\\ \dot{\varphi}(t)=\dfrac{\mathrm{d}\varphi}{\mathrm{d}t}=a_0+a_1t+\dfrac{a_2}{2}t^2,\\ \ddot{\varphi}(t)=\dfrac{\mathrm{d}^2\varphi}{\mathrm{d}\varphi^2}=a_1+a_2t.\end{cases} \tag{26}$$

By means of which, we can rewrite (25) as

$$\mathrm{LPP}_x^3(t,\bar{w})\mid_{w_2=a_2}=\frac{2A^2\sqrt{\pi}\cdot\mathrm{e}^{-\frac{(w-\dot{\varphi})^2}{\alpha+\frac{1}{\alpha}(w_1-\ddot{\varphi})^2}}}{\sqrt{\alpha+\frac{1}{\alpha}(w_1-\ddot{\varphi})^2}}. \tag{27}$$

We can denote by χ the concentrated domain for which the 3 dB bandwidth condition is fulfilled

$$\begin{aligned}\chi&=\{(t,\bar{w})\mid_{w_2=a_2}\!:\mathrm{LPP}_x^3(t,\bar{w})\mid_{w_2=a_2}^{3\ \mathrm{dB}}\geqslant 0.5\ \ \max\mathrm{LPP}_x^3(t,\bar{w})\}\\&=\left\{(t,\bar{w})\mid_{w_2=a_2}\!:\mathrm{LPP}_x^3(t,\bar{w})\mid_{w_2=a_2}\geqslant 0.5\cdot 2A^2\sqrt{\frac{\pi}{\alpha}}\right\}.\end{aligned} \tag{28}$$

$\mathrm{LPP}_x^3(t,\bar{w})\mid_{w_2=a_2}^{3\ \mathrm{dB}}$ in (28) represents a surface given by

$$\mathrm{LPP}_x^3(t,\bar{w})\mid_{w_2=a_2}^{3\ \mathrm{dB}}=\frac{2A^2\sqrt{\pi}\cdot\mathrm{e}^{-\frac{(w-\dot{\varphi})^2}{\alpha+\frac{1}{\alpha}(w_1-\ddot{\varphi})^2}}}{\sqrt{\alpha+\frac{1}{\alpha}(w_1-\ddot{\varphi})^2}}\geqslant\frac{1}{2}2A^2\sqrt{\frac{\pi}{\alpha}}, \tag{29}$$

whose maximum is attained when $w=\dot{\varphi}$ and $w_1=\ddot{\varphi}$. The equal sign in (29) determines the equation of the boundary line C at the bottom of the surface (see Figure 1). By setting the coordinates for points P_1 and P_2 in (29) we can straightforward determine the limits of δ and δ_1 as

$$\begin{cases}\delta\mid_{P_1}=\sqrt{\alpha\ln 2},\\ \delta_1\mid_{P_2}=\sqrt{3}\alpha,\end{cases} \tag{30}$$

and based on the symmetry of the surface contour we arrive to the following concentrated domain:

$$\begin{cases}\chi_w=\{w:\dot{\varphi}(t)-\sqrt{\alpha\ln 2}\leqslant w\leqslant\dot{\varphi}(t)+\sqrt{\alpha\ln 2}\},\\ \chi_{w_1}=\{w_1:\ddot{\varphi}(t)-\sqrt{3}\alpha\leqslant w_1\leqslant\ddot{\varphi}(t)+\sqrt{3}\alpha\}.\end{cases} \tag{31}$$

Note that the concentrated domain χ is not an exhaustive domain because we have constrained it to be bounded to $w_2=a_2$. That means that one supreme domain $\chi_{\sup}(t,\bar{w})\supset\chi$ exists

$$\chi_{\sup}=\{(t,\bar{w}):\mathrm{LPP}_x^3(t,\bar{w})>0.5\ \ \max\mathrm{LPP}_x^3(t,\bar{w})\}, \tag{32}$$

that fulfills the condition in (32) where w_2 is a free variable.

We have found this way the boundaries of a region in the frequency domain $w,w_1,w_2=a_2$ inside the 3 dB bandwidth limits for any time t of the QFM signal. Eq. (31) defines these limits.

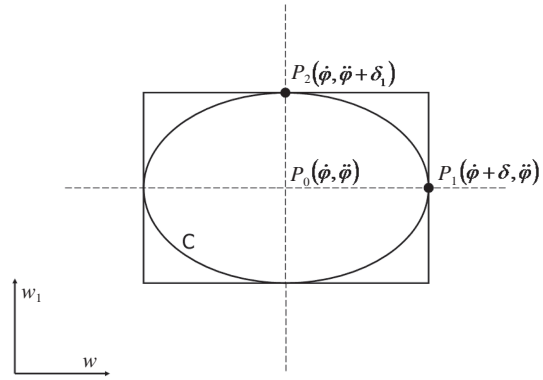

Figure 1 Geometry of the problem. Points P_1 and P_2 determine the limits of the rectangular area enclosing the baseline of the 3 dB surface and P_0 is the position of the maximum.

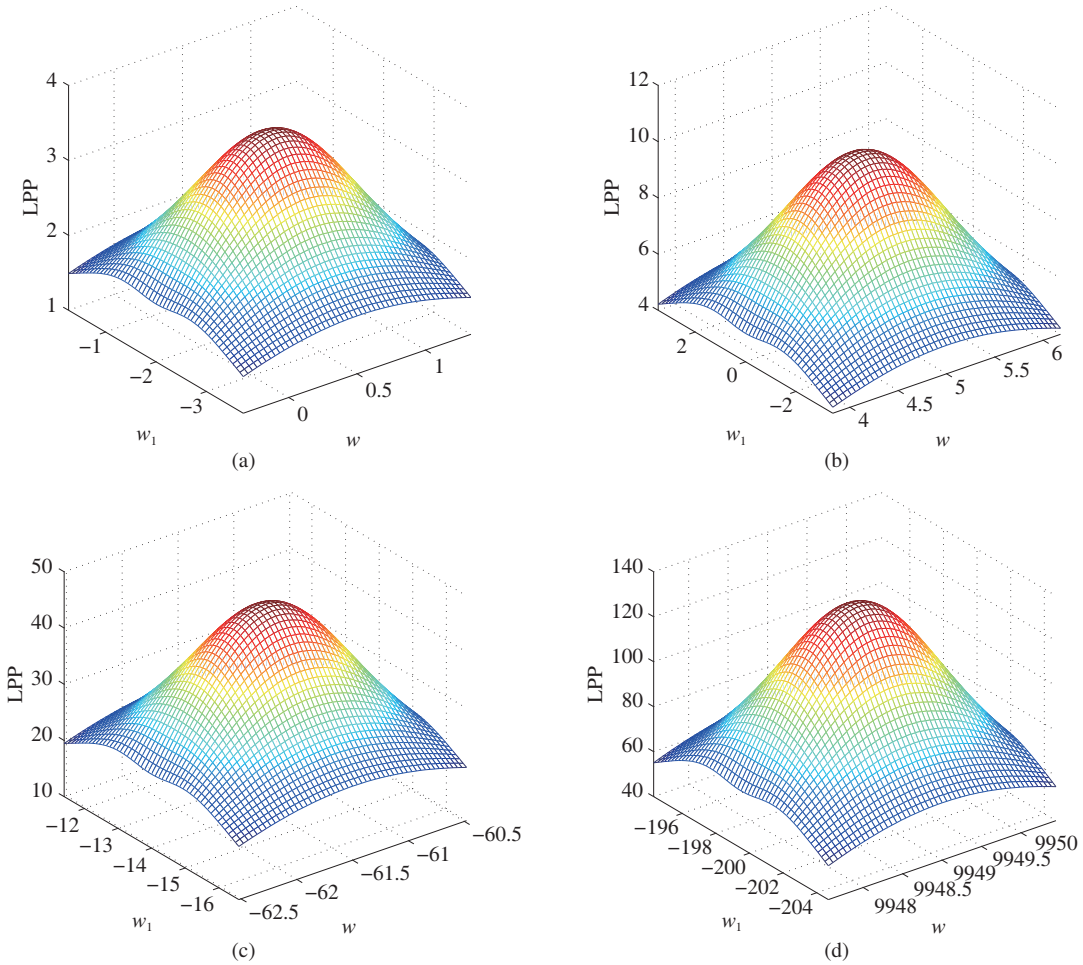

Figure 2 (Color online) Examples of LPP 3 dB bandwidth for different input parameters of the QFM signal. (a) $t = 0$, $A = 1, a_0 = 0.5, a_1 = -2, a_2 = -1, \alpha = 1$; (b) $t = 2, A = 2, a_0 = 1, a_1 = 4, a_2 = -2, \alpha = 2$; (c) $t = 10, A = 4, a_0 = 3.5, a_1 = 1, a_2 = -1.5, \alpha = 1.5$; (d) $t = -100, A = 8, a_0 = -1, a_1 = 0.5, a_2 = 2, \alpha = 3$.

Based on (31), Figure 2 presents four examples of the $\mathrm{LPP}_x^3(t,\bar{w})\,|_{w_2=a_2}^{3\ \mathrm{dB}}$ using different values of the optional parameters of the QFM signal.

Theorem 3. The 3 dB SNR in the LPFT domain for the QFM signal $x(t)$ is determined by the

parameter α when the SNR_t is given. The relationship between $\mathrm{SNR}^{3\ \mathrm{dB}}_{\mathrm{LPFT}}$ and α is

$$\mathrm{SNR}^{3\ \mathrm{dB}}_{\mathrm{LPFT}} = 1.32\sqrt{\frac{\pi}{\alpha}}\mathrm{SNR}_t. \tag{33}$$

Proof. Eq. (18) establishes that the LPP^3_x cannot vanished when t tends to infinity, because for any value of $-\infty < t < \infty$ there are values of w, w_1, w_2 that satisfy the required conditions to reach the upper limit. However, we can calculate the average power of the 3 dB LPP^3_x for any time position t. In general, the average value of an arbitrary continuous signal $f(x)$ is given by $\overline{f(x)} = \frac{1}{b-a}\int_a^b f(x)\mathrm{d}x$. Consequently, the average power of the signal $\mathrm{LPP}^3_x(t,\bar{w})\,|^{3\ \mathrm{dB}}_{w_2=a_2}$ at time t is by the following definition:

$$\overline{\underset{(t,\bar{w})\in\chi}{\mathrm{LPP}^3_x}}(t,\bar{w})\,|^{3\ \mathrm{dB}}_{w_2=a_2} = \frac{1}{|\chi_{w_1}|}\int_{\mathrm{LL}_1}^{\mathrm{LL}_2}\frac{1}{|\chi_w|}\int_{L_1}^{L_2}\frac{2A^2\sqrt{\pi}\cdot \mathrm{e}^{-\frac{(w-\dot{\varphi})^2}{\alpha+\frac{1}{\alpha}(w_1-\dot{\varphi})^2}}}{\sqrt{\alpha+\frac{1}{\alpha}(w_1-\ddot{\varphi})^2}}\mathrm{d}w\mathrm{d}w_1, \tag{34}$$

and the limits of integrations are defined as per (31). That means, $|\chi_w| = 2\sqrt{\alpha\ln 2}$, $|\chi_{w_1}| = 2\sqrt{3}\alpha$, $L_1 = \dot{\varphi}(t) - \sqrt{\alpha\ln 2}$, $L_2 = \dot{\varphi}(t) + \sqrt{\alpha\ln 2}$, $\mathrm{LL}_1 = \ddot{\varphi}(t) - \sqrt{3}\alpha$, $\mathrm{LL}_2 = \ddot{\varphi}(t) + \sqrt{3}\alpha$, and leads to

$$\overline{\underset{(t,\bar{w})\in\chi}{\mathrm{LPP}^3_x}}(t,\bar{w})\,|^{3\ \mathrm{dB}}_{w_2=a_2} = \frac{1}{|\chi_{w_1}|}\int_{\mathrm{LL}_1}^{\mathrm{LL}_2}\frac{1}{|\chi_w|}\int_{L_1}^{L_2}\frac{2A^2\sqrt{\pi}\cdot \mathrm{e}^{-\frac{(w-\dot{\varphi})^2}{\alpha+\frac{1}{\alpha}(w_1-\dot{\varphi})^2}}}{\sqrt{\alpha+\frac{1}{\alpha}(w_1-\ddot{\varphi})^2}}\mathrm{d}w\mathrm{d}w_1. \tag{35}$$

Let us consider first the integral $I = \int_{L_1}^{L_2}\frac{1}{m}\cdot \mathrm{e}^{-\frac{(w-\dot{\varphi})^2}{m^2}}\mathrm{d}w$, where we have called $m = \sqrt{\alpha+\frac{1}{\alpha}(w_1-\ddot{\varphi})^2}$. By making $u = \frac{w-\dot{\varphi}}{m}$, then $\mathrm{d}w = m\cdot\mathrm{d}u$ and I becomes $I = \int_{-\frac{1}{m}\sqrt{\alpha\ln 2}}^{\frac{1}{m}\sqrt{\alpha\ln 2}}\mathrm{e}^{-u^2}\mathrm{d}u$. This integral does not have an algebraic representation and requires to be evaluated by means of the error function, defined as $\mathrm{erf}(z) \equiv (1/\sqrt{\pi})\int_{-z}^{z}\mathrm{e}^{-x^2}\mathrm{d}x$ and then we write

$$I = \int_{-\frac{1}{m}\sqrt{\alpha\ln 2}}^{\frac{1}{m}\sqrt{\alpha\ln 2}}\mathrm{e}^{-u^2}\mathrm{d}u = \sqrt{\pi}\left(\mathrm{erf}\left(\frac{\sqrt{\alpha\ln 2}}{\sqrt{\alpha+\frac{1}{\alpha}(w_1-\ddot{\varphi})^2}}\right)\right). \tag{36}$$

Substituting this result in (35) we get

$$\overline{\underset{(t,\bar{w})\in\chi}{\mathrm{LPP}^3_x}}(t,\bar{w})\,|^{3\ \mathrm{dB}}_{w_2=a_2} = \frac{A^2\pi}{2\alpha\sqrt{3\alpha\ln 2}}\int_{\ddot{\varphi}-\sqrt{3}\alpha}^{\ddot{\varphi}+\sqrt{3}\alpha}\mathrm{erf}\left(\frac{\sqrt{\alpha\ln 2}}{\sqrt{\alpha+\frac{1}{\alpha}(w_1-\ddot{\varphi})^2}}\right)\mathrm{d}w_1. \tag{37}$$

By the change of variable, $u = w_1 - \ddot{\varphi}$, the integral in (37) becomes

$$\overline{\underset{(t,\bar{w})\in\chi}{\mathrm{LPP}^3_x}}(t,\bar{w})\,|^{3\ \mathrm{dB}}_{w_2=a_2} = \frac{A^2\pi}{2\alpha\sqrt{3\alpha\ln 2}}\int_{-\sqrt{3}\alpha}^{\sqrt{3}\alpha}\mathrm{erf}\left(\frac{\sqrt{\alpha\ln 2}}{\sqrt{\alpha+\frac{1}{\alpha}u^2}}\right)\mathrm{d}u. \tag{38}$$

An approximated solution to integral (38) can be found by subdividing the span of integration in sub-intervals Δu and summing up the elemental results. That is

$$\overline{\underset{(t,\bar{w})\in\chi}{\mathrm{LPP}^3_x}}(t,\bar{w})\,|^{3\ \mathrm{dB}}_{w_2=a_2} \cong \frac{A^2\pi}{2\alpha\sqrt{3\alpha\ln 2}}\sum_{u=-\sqrt{3}\alpha}^{u=+\sqrt{3}\alpha}\mathrm{erf}\left(\frac{\sqrt{\alpha\ln 2}}{\sqrt{\alpha+\frac{1}{\alpha}u^2}}\right)\Delta u, \tag{39}$$

where $\Delta u = 2\sqrt{3}\alpha/N$, for $N+1$ subintervals of integration. Table 1 summarizes the results for the examples in Figure 2.

One important experimental finding is that

$$\overline{\underset{(t,\bar{w})\in\chi}{\mathrm{LPP}^3_x}}(t,\bar{w})\,|^{3\ \mathrm{dB}}_{w_2=a_2} = 0.66\cdot\max_{(t,w)}\mathrm{LPP}^3_x(t,\bar{w}) = 1.32A^2\sqrt{\frac{\pi}{\alpha}}. \tag{40}$$

Table 1 Numerical results for $\mathrm{LPP}_x^3(t,\bar{w})\,|_{w_2=a_2}^{3\ \mathrm{dB}}$ examples in Figure 2

Example	t	A	a_0	a_1	a_2	α	P_0	P_1	P_2	Average	Avg/P_0
I	0	1	0.5	−2	−1	1	3.54	1.77	1.77	2.34	0.66
II	2	2	1	4	−2	2	10.03	5.01	5.01	6.63	0.66
III	10	4	3.5	1	−1.5	1.5	46.31	23.16	23.16	30.62	0.66
IV	−100	8	−1	0.5	2	3	130.99	65.49	65.49	86.60	0.66

The mean power of noise $\eta(t)$ in the LPFT domain is

$$\overline{\underset{(t,\bar{w})\in\chi}{\mathrm{LPP}_\eta^3}} = \mathrm{E}\left|\int \eta(t+\tau)h^*(\tau)\mathrm{e}^{-\mathrm{j}(w\tau+\frac{w_1}{2}\tau^2+\frac{w_2}{3!}\tau^3)}\mathrm{d}\tau\right|^2 = \sigma^2.$$

By defining SNR_t as the SNR in time domain, that is given by A^2/σ^2, then the $\mathrm{SNR}^{3\ \mathrm{dB}}$ of a QFM signal in the LPFT domain when $w_2 = a_2$ can be approximated as

$$\mathrm{SNR}_{\mathrm{LPFT}}^{3\ \mathrm{dB}} = \frac{\overline{\underset{(t,\bar{w})\in\chi}{\mathrm{LPP}_x^3}}(t,\bar{w})\,|_{w_2=a_2}^{3\ \mathrm{dB}}}{\overline{\underset{(t,\bar{w})\in\chi}{\mathrm{LPP}_\eta^3}}(t,\bar{w})} \cong 1.32\sqrt{\frac{\pi}{\alpha}}\mathrm{SNR}_t. \tag{41}$$

It can be seen from (41) that the SNR of QFM signal $x(t)$ in the LPFT domain is related to the window function parameter α and is independent of the other variables. The SNR is inversely proportional to the window function parameter, i.e., SNR will increase when α is smaller. Especially when $\alpha < (1.32)^2\pi = 5.47$, the SNR in the LPFT domain performs better than that in the time domain. When α limits to 0, SNR approaches toward infinity. However, the window function has to keep stationary feature in the local domain, so it cannot achieve infinity. As a result, it has been found that the LPFT indeed improve the SNR of the QFM signal.

4 Simulation results

In this section, simulation experiments are performed to verify above derived theorems, and analysis results of 3 dB SNR in the LPFT domain are graphically compared with that in the LCT domain. To illustrate the simulation process, the following example is considered.

A single QFM signal with parameters $a_0 = 3$, $a_1 = -2$, and $a_2 = 0.5$ is given as follows:

$$x(t) = \mathrm{e}^{\mathrm{j}(3t-t^2+\frac{1}{12}t^3)}. \tag{42}$$

The SNR in the time domain is given as $\mathrm{SNR}_t = -3$ dB. We know that the instantaneous energy of $x(t)$ arrives maximum varying with w_1. But, the theoretical result in Theorem 3 shows that it has no relationship with other parameters except for Gaussian window parameter α under a given SNR_t. In order to verify the above theorems, we use the 3rd order LPFT whose parameters are (w_1, w_2) to deal with $x(t)$.

Firstly, the influence of the LPFT parameters and window parameter to the SNR in the LPFT domain is given in Figure 3. Figure 3(a) shows that the relationship between w_1 and $\mathrm{SNR}_{\mathrm{LPFT}}^{3\ \mathrm{dB}}$ under $w_2 = a_2$, where the sampling interval of t and w is 10 and 40, respectively. Five solid blue color lines means how $\mathrm{SNR}_{\mathrm{LPFT}}^{3\ \mathrm{dB}}$ varies with w_1 when α equals to 0.5, 0.75, 1, 1.25, and 1.5, respectively. The red lines represent the theoretical value in Theorem 3, i.e., $\mathrm{SNR}_{\mathrm{LPFT}}^{3\ \mathrm{dB}} \cong 1.32\sqrt{\frac{\pi}{\alpha}}\mathrm{SNR}_t$, under different α. It concludes that the simulation results almost coincide with the theoretical values, which further states that $\mathrm{SNR}_{\mathrm{LPFT}}^{3\ \mathrm{dB}}$ has no relationship with w_1. Besides, from Figure 3(a), it is clearly to see that $\mathrm{SNR}_{\mathrm{LPFT}}^{3\ \mathrm{dB}}$ increases with the decrease of α. This relationship between α and $\mathrm{SNR}_{\mathrm{LPFT}}^{3\ \mathrm{dB}}$ is then shown in Figure 3(b) and simulation experiment fits the theoretical results well for $\alpha \in (0, 6)$. In other words, it is an inverse function between α and $\mathrm{SNR}_{\mathrm{LPFT}}^{3\ \mathrm{dB}}$. In addition, when $\alpha < 5.5$, the line of $\mathrm{SNR}_{\mathrm{LPFT}}^{3\ \mathrm{dB}}$ is above of SNR_t. That is to say,

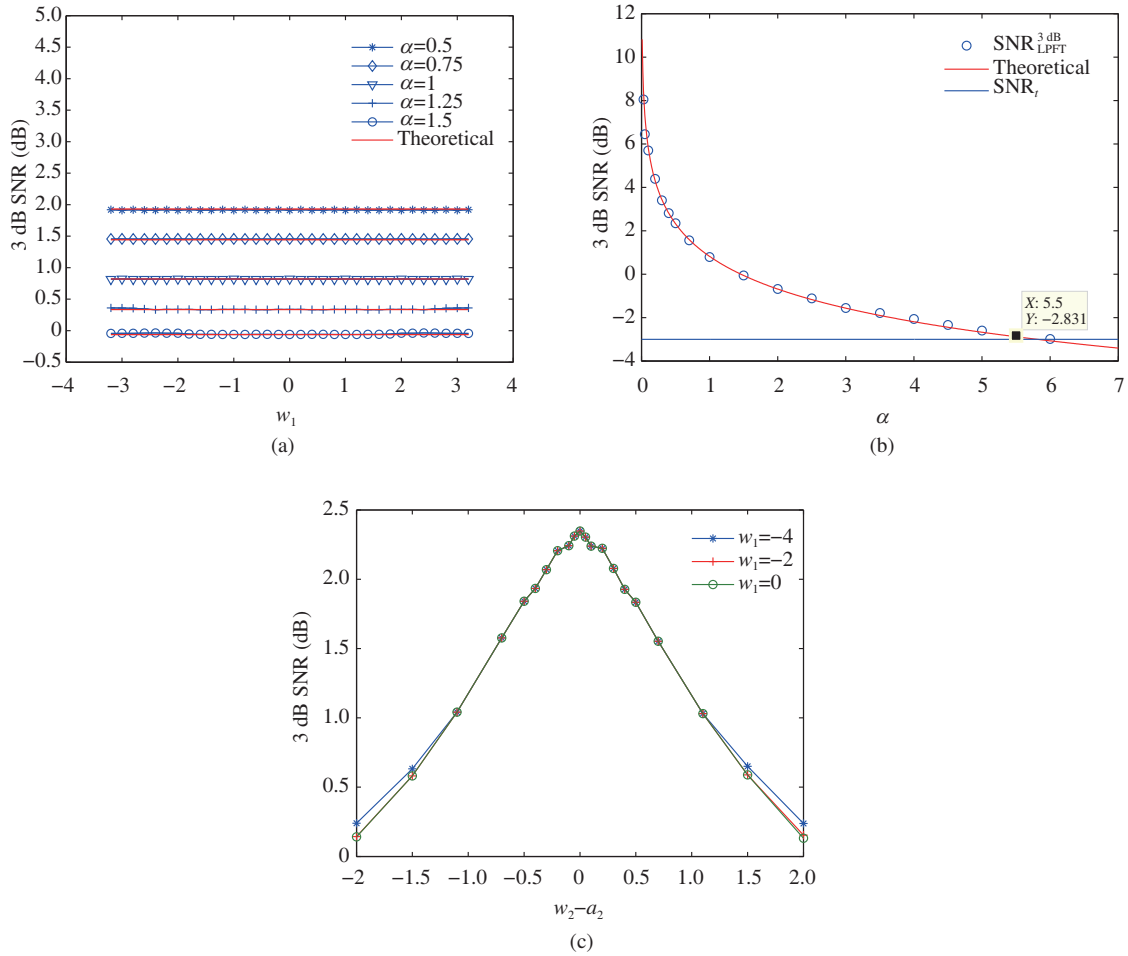

Figure 3 (Color online) (a) The relation between $\mathrm{SNR}^{3\ \mathrm{dB}}_{\mathrm{LPFT}}$ and LPFT parameter w_1; (b) the relation between $\mathrm{SNR}^{3\ \mathrm{dB}}_{\mathrm{LPFT}}$ and Gaussian window parameter α; (c) the relation between $\mathrm{SNR}^{3\ \mathrm{dB}}_{\mathrm{LPFT}}$ and $w_2 - a_2$.

under this condition, the performance of a QFM signal in the LPFT domain is much better than that in the time domain. Next, the relationship between w_2 and $\mathrm{SNR}^{3\ \mathrm{dB}}_{\mathrm{LPFT}}$ is demonstrated in Figure 3(c). Here, three curve lines stand for $\mathrm{SNR}^{3\ \mathrm{dB}}_{\mathrm{LPFT}}$ varying with w_2 when w_1 equals to -4, -2, and 0, respectively. From these results, we conclude that $\mathrm{SNR}^{3\ \mathrm{dB}}_{\mathrm{LPFT}}$ is increasing when w_2 limits to a_2 for different values of w_1, and it reaches maximum when $w_2 = a_2$, independent to w_1. It satisfies with the constraint condition in corresponding theorems well.

Besides, it is well-known that the LCT is a powerful tool to analyze non-stationary signals encountered in many realistic situations. The 3 dB SNR analysis in the corresponding domain have verified quantitatively that the LCT can achieve a better level than time domain, STFT domain and WVD domain for the same signal [18]. In order to verify the performance of a QFM signal corrupted with noise in the LCT and LPFT domain, a ratio between $\mathrm{SNR}^{3\ \mathrm{dB}}_{\mathrm{LPFT}}$ and $\mathrm{SNR}^{3\ \mathrm{dB}}_{\mathrm{LCT}}$ is under consideration. According to the definition of the LCT, the mean power has nothing to do with the parameter d [18], which states that only (a, b) effects the SNR. For the sake of simplicity, we fixed d, for example, $d = 1$. By giving different values a, b (Herein, let the ratio of a, b be a constant denoted as k), $\mathrm{SNR}^{3\ \mathrm{dB}}_{\mathrm{LCT}}$ can be obtained in the same way as $\mathrm{SNR}^{3\ \mathrm{dB}}_{\mathrm{LPFT}}$. The process is stated as follows. First of all, the LCT of a QFM signal is obtained under some given parameters (a, b) and Gaussian window. Then, the 3 dB bandwidth of signal is gained by the maximum of spectrum in the LCT domain under the definition in (9). Lastly, according to 3 dB mean power of the signal and noise, the 3 dB LCT-typed SNR of a QFM signal is carried out via numerical experiment. By using the same Gaussian window function with parameter $\alpha = 0.25$, the

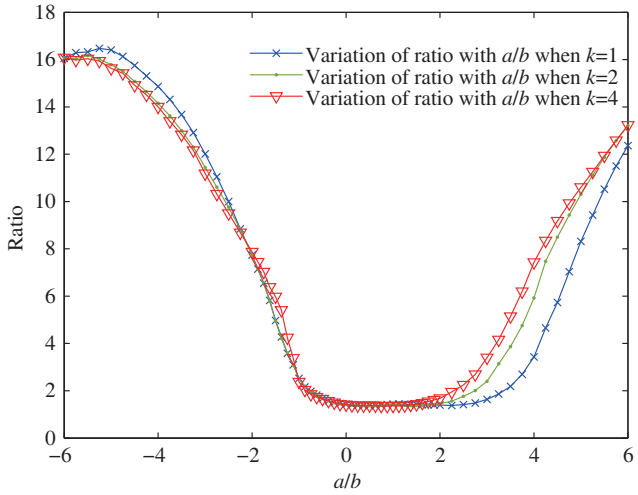

Figure 4 (Color online) The ratio between $\mathrm{SNR}^{3\ \mathrm{dB}}_{\mathrm{LPFT}}$ and $\mathrm{SNR}^{3\ \mathrm{dB}}_{\mathrm{LCT}}$ versus a/b

ratio between $\mathrm{SNR}^{3\ \mathrm{dB}}_{\mathrm{LPFT}}$ and $\mathrm{SNR}^{3\ \mathrm{dB}}_{\mathrm{LCT}}$ is given by

$$\mathrm{Ratio} = \frac{\mathrm{SNR}^{3\ \mathrm{dB}}_{\mathrm{LPFT}}}{\mathrm{SNR}^{3\ \mathrm{dB}}_{\mathrm{LCT}}} = \frac{\overline{\underset{(t,\bar{w})\in\chi_1}{\mathrm{LPP}^3_x}\,(t,\bar{w})}}{\overline{\underset{(t,u)\in\chi_2}{|\mathrm{LCT}^A_x|^2}(t,u)}}. \tag{43}$$

Figure 4 shows three different plots in which how Ratio varies with the LCT parameters (a,b). Even though $\mathrm{SNR}^{3\ \mathrm{dB}}_{\mathrm{LCT}}$ is much different when the (a,b) is not the same, but Ratio is always larger than 1. That is to say, $\mathrm{SNR}^{3\ \mathrm{dB}}_{\mathrm{LPFT}}$ is always greater than $\mathrm{SNR}^{3\ \mathrm{dB}}_{\mathrm{LCT}}$, which quantitatively verifies that the QFM signal $x(t)$ has an improvement on time-frequency energy concentration ability in the LPFT domain than that of the LCT domain.

5 Application

In this section, we give a parameter estimation application to show the performance of the LPFT and the LCT for a QFM signal under noise environment. As mentioned in Theorem 1, for a QFM signal, the LPFT arrives the maximum under the condition in (18). For the sake of simplicity, we consider the LPFT when $t = 0$, then the principle of parameter estimation of a given QFM signal can be stated as follows:

$$\{\hat{a}_0, \hat{a}_1, \hat{a}_2\} = \arg \max_{w,w_1,w_2} \mathrm{LPP}^3_x(0,\bar{w}). \tag{44}$$

It means that by searching the peak of the LPP in the whole three-dimension space of w, w_1, w_2, parameters of a given QFM signal can be estimated in accordance to the position information of the its peak. Herein, the global search method in the whole three-dimension space is used to locate the peak of the LPP.

In this experiment, the model of a QFM signal are sampled as

$$x(n) = W_N^{-(rn+ln^2+mn^3)}, \quad 0 \leqslant n \leqslant N-1, \tag{45}$$

where r, l, m represent the constant frequency, first chirp rate and second chirp rate, respectively. N means the length of signal $x(n)$. A signal $x(n)$ corrupted with noise is given as

$$y(n) = x(n) + \eta(n), \quad 0 \leqslant n \leqslant N-1, \tag{46}$$

where $\eta(n)$ denotes the white Gaussian noise. It is noted that LPP varies over w, w_1, w_2. The simulation results are then presented in the $w - w_1$ plane, $w - w_2$ plane, and $w_1 - w_2$ plane, respectively.

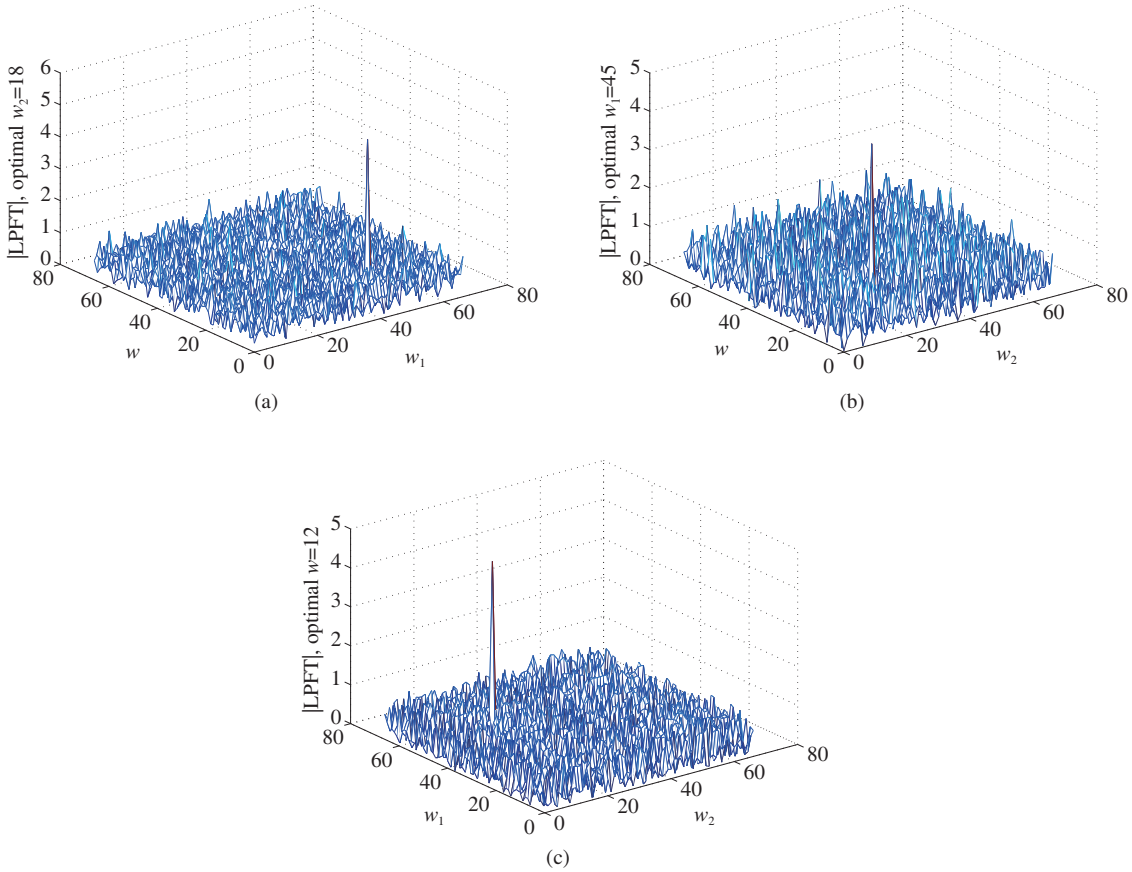

Figure 5 (Color online) LPP of a QFM signal in the noise environment $y(n)$ in (a) $w-w_1$ plane under optimal $w_2=18$, (b) $w-w_2$ plane under optimal $w_1=45$, and (c) w_1-w_2 plane under optimal $w=12$.

Following the method in (44), we show the results of parameter estimation for signal $y(n)$ in Figure 5. The SNR in the time domain here is -10 dB. The parameters of the QFM signal are $(r,l,m)=(12,45,18)$ and $N=67$. Based on the relationship between LPFT-related 3 dB SNR and Gaussian window parameter in Figure 3(b), we choose $\alpha=0.5$ to achieve better local performance. As shown in Figures 5(a)–(c), a peak can be detected clearly through a global search in the three-dimension space. Figure 5(a) shows that under the optimal parameter $w_2=18$, the peak of LPP is located in $(w,w_1)=(12,45)$. Figure 5(b) shows that under the optimal parameter $w_1=45$, the peak of LPP is located in $(w,w_2)=(12,18)$. Figure 5(c) shows that under the optimal parameter $w=12$, the peak of LPP is located in $(w_1,w_2)=(45,18)$. It is indicated that the parameters of the signal $x(n)$ can be estimated exactly based the LPFT.

In the following, we use the LCT to process the same noisy QFM signal $y(n)$ used by the LPFT. In Figure 6, the LCT spectrum is plotted in the LCT frequency u and parameter-ratio $k=a/b$ plane. In Figure 6, no peak can be detected from the LCT spectrum. To make it clearly, we project it into the u axis in Figure 7(a) and parameter-ratio k axis in Figure 7(b), respectively. Compared with the results related to the LPFT, it is hard to estimate the parameters of the given QFM signal by searching the peak directly like the LPFT. Such observations are expected because the use of the LPFT can further improve the SNR more effectively than those of the LCT, just indicated by our previous analysis.

Furthermore, another experiment is carried out to show the accuracy of the LPFT-based method via the comparison between the estimated results in terms of mean square error (MSE) and the Cramer-Rao lower bound (CRLB) through Monte-Carlo simulation. In this experiment, the parameters of the QFM signal are $a_0=12.3, a_1=45.2, a_2=18.1$. The length of discrete signal and window parameter are same as above. The scope of the input SNR varies from -15 to 15 dB with a step of 2 dB. For each SNR the Monte-Carlo runs 100 independent experiments. Figure 8 shows the final estimated consequences compared with the CRLB, respectively. The overall trend of the MSEs of different parameters is to

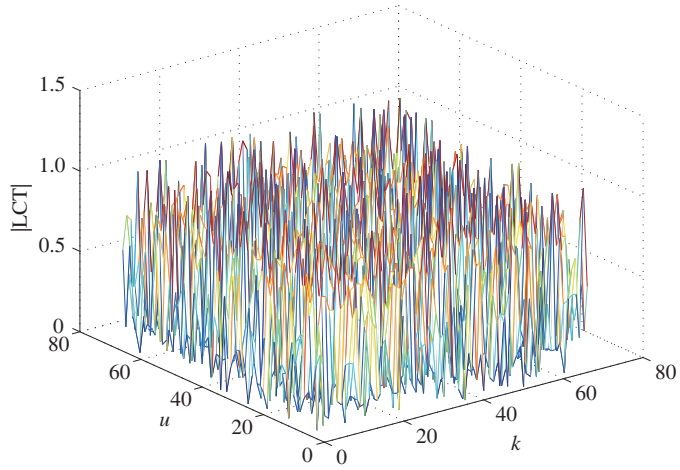

Figure 6 (Color online) LCT spectrum of a QFM signal in the noise environment $y(n)$ in $u-k$ plane.

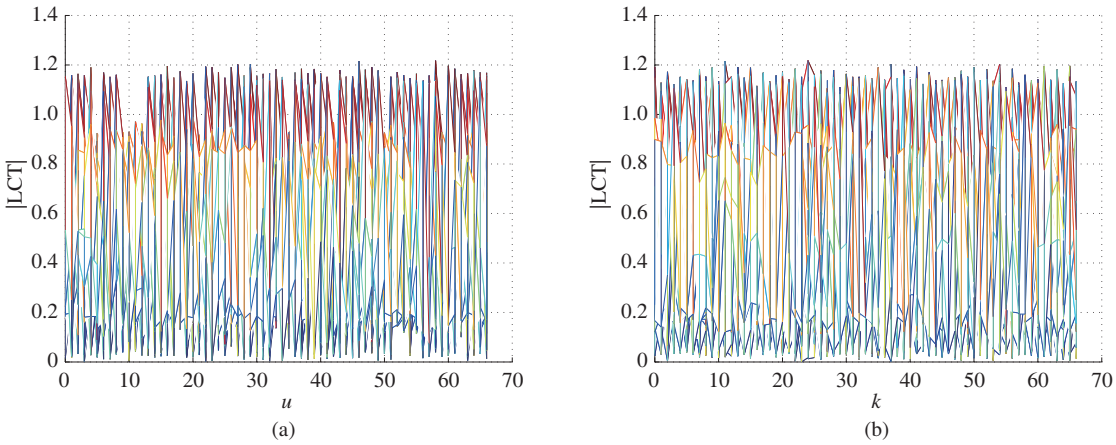

Figure 7 (Color online) LCT of a QFM signal in the noise environment $y(n)$ projected in (a) LCT-frequency u axis, (b) parameter-ratio k axis.

decrease with increasing SNR, whereas under some SNR environment, the MSEs tend to stable and are above the CRLB, respectively.

It is noted that the computational burden of the LPFT-based method is increased through a global search. It can be reduced by several approaches: on the one hand, fast algorithms of the LPFT can be considered in the real applications [17]; one the other hand, optimization algorithms can be used to replace the global research and further reduce the computational complexity of parameter estimation. In summary, since the noise widely exists in most areas of real world, the quantitative SNR analysis is an important research issue. It is not only a useful measure to evaluate the performance of different TF distributions, but also offers a significant guidance purpose under real requirements.

6 Conclusion

In this paper, a quantitative SNR analysis of a QFM signal in the LPFT domain with Gaussian window function has been carried out. Because the conventional SNR definition cannot explain the relationship with bandwidth, 3 dB SNR given by Xia are utilized. In order to do so, three valuable theorems are proposed and well proofed. Theorem 1 shows the peak value of instantaneous energy is maximum under $w_2 = a_2$ when the QFM signal is transformed by 3rd order LPFT. Theorem 2 analyzes the 3 dB bandwidth of QFM signal in the LPFT domain and some specific examples are given. The quantitative SNR analysis is derived in Theorem 3. We ultimately show that the 3 dB SNR based on the LPFT with Gaussian

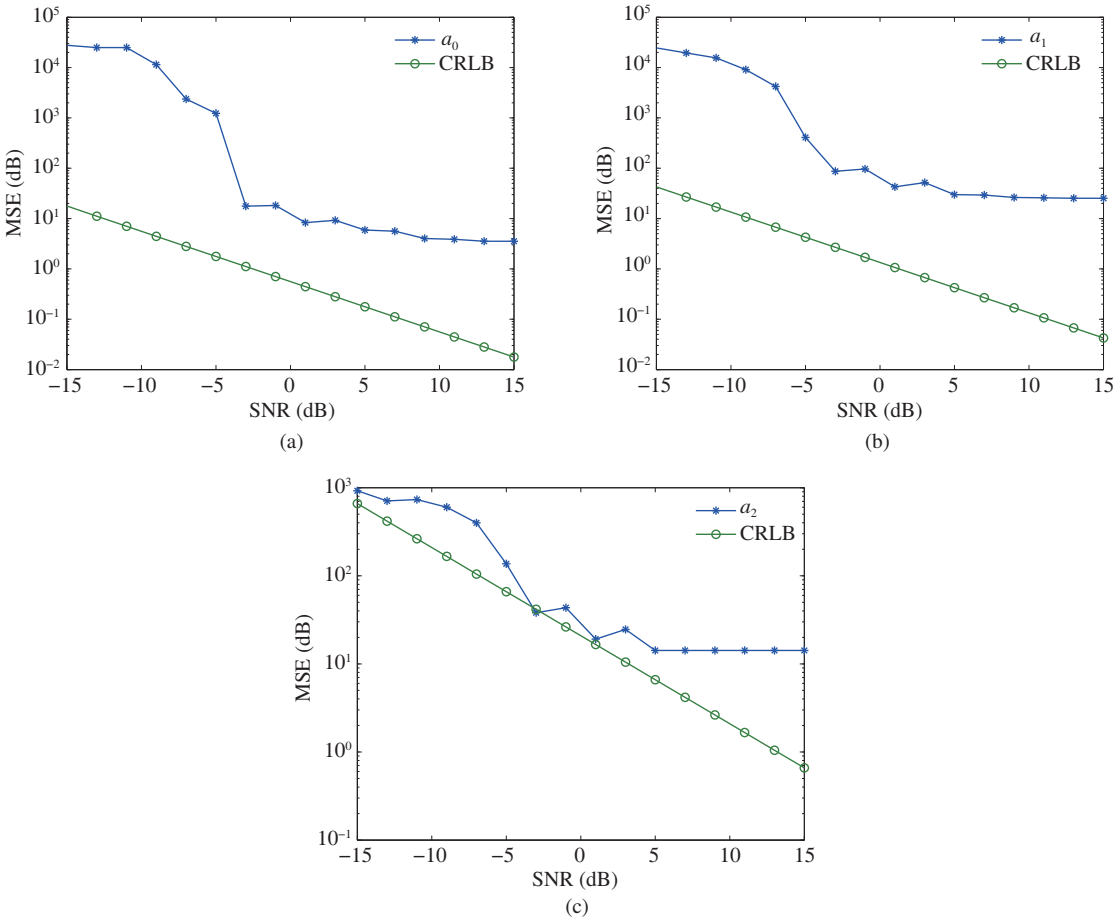

Figure 8 (Color online) MSEs of the parameter estimations via LPFT-based method. (a) Constant frequency a_0; (b) first chirp rate a_1; (c) second chirp rate a_2.

window is closely related with window parameter under a given time-related SNR, independent with other variables. And a comparison between the performance of the LPFT and LCT is given in simulations as well. This work is significantly in practical application to show the TFRs' characteristics in terms of SNR. In the future, we will further focus on how to improve the accuracy of parameter estimation and reduce the computation load via LPFT-based method.

Acknowledgements This work was supported by National Natural Science Foundation of China (Grant No. 61671063), and also by Foundation for Innovative Research Groups of National Natural Science Foundation of China (Grant No. 61421001).

References

1 Wang J Z, Su S Y, Chen Z P. Parameter estimation of chirp signal under low SNR. Sci China Inf Sci, 2015, 58: 020307
2 Cohen L. Time-frequency distributions-a review. Proc IEEE, 1989, 77: 941–981
3 Whitelonis N, Ling H. Radar signature analysis using a joint time-frequency distribution based on compressed sensing. IEEE Trans Antenn Propagat, 2014, 62: 755–763
4 Chen V C, Ling H. Joint time-frequency analysis for radar signal and image processing. IEEE Signal Process Mag, 1999, 16: 81–93
5 Pitton J W, Wang K S, Juang B H. Time-frequency analysis and auditory modeling for automatic recognition of speech. Proc IEEE, 1996, 84: 1199–1215
6 Amin M G. Interference mitigation in spread spectrum communication systems using time-frequency distributions. IEEE Trans Signal Process, 1997, 45: 90–101
7 Xia X-G. A quantitative analysis of SNR in the short-time Fourier transform domain for multicomponent signals. IEEE Trans Signal Process, 1998, 46: 200–203

8 Bai G, Tao R, Zhao J, et al. Fast FOCUSS method based on bi-conjugate gradient and its application to space-time clutter spectrum estimation. Sci China Inf Sci, 2017, 60: 082302
9 Mu W F, Amin M G. SNR analysis of time-frequency distributions. In: Proceedings of IEEE International Conference on Acoustics, Speech, and Signal Processing (ICASSP), Turkey, 2000. II645–II648
10 Li X M, Bi G A, Ju Y T. Quantitative SNR analysis for ISAR imaging using LPFT. IEEE Trans Aerosp Electron Syst, 2009, 45: 1241–1248
11 Xia X-G, Wang G Y, Chen V C. Quantitative SNR analysis for ISAR imaging using joint time-frequency analysis-short time Fourier transform. IEEE Trans Aerosp Electron Syst, 2002, 38: 649–659
12 Stankovic L, Ivanovic V, Petrovic Z. Unified approach to noise analysis in the Wigner distribution and spectrogram. Ann Telecommun, 1996, 11: 585–594
13 Stankovic L, Stankovic S. Wigner distribution of noisy signals. IEEE Trans Signal Process, 1993, 41: 956–960
14 Ouyang X, Amin M G. Short-time Fourier transform receiver for nonstationary interference excision in direct sequence spread spectrum communications. IEEE Trans Signal Process, 2001, 49: 851–863
15 Song J, Niu Z Y, Zhang J Y. OFD-LFM signal design and performance analysis for distributed aperture fully coherent radar. Sci China Inf Sci, 2015, 45: 968–984
16 Xia X-G, Chen V C. A quantitative SNR analysis for the pseudo Wigner-Ville distribution. IEEE Trans Signal Process, 1999, 47: 2891–2894
17 Li X M, Bi G, Stankovic S, et al. Local polynomial Fourier transform: a review on recent developments and applications. Signal Process, 2011, 91: 1370–1393
18 Wu Y, Li B Z, Cheng Q Y. A quantitative SNR analysis of LFM signals in the linear canonical transform domain with Gaussian windows. In: Proceedings of IEEE International Conference on Mechatronic Sciences, Electric Engineering and Computer (MEC), Shengyang, 2013. 1426–1430
19 Li Y, Liu K, Tao R, et al. Adaptive viterbi-based range-instantaneous Doppler algorithm for ISAR imaging of ship target at sea. IEEE J Ocean Eng, 2015, 40: 417–425
20 O'Shea P. A fast algorithm for estimating the parameters of a quadratic FM signal. IEEE Trans Signal Process, 2004, 52: 385–393
21 Bai X, Tao R, Wang Z, et al. ISAR imaging of a ship target based on parameter estimation of multicomponent quadratic frequency-modulated signals. IEEE Trans Geosci Remote Sens, 2014, 52: 1418–1429
22 Wang Y, Zhao B. Inverse synthetic aperture radar imaging of nonuniformly rotating target based on the parameters estimation of multicomponent quadratic frequency-modulated signals. IEEE Sens J, 2015, 15: 4053–4061
23 Katkovnik V. Discrete-time local polynomial approximation of the instantaneous frequency. IEEE Trans Signal Process, 1998, 46: 2626–2637
24 Djurović I, Thayaparan T, Stanković L. Adaptive local polynomial Fourier transform in ISAR. EURASIP J Adv Signal Process, 2006, 2006: 36093
25 Katkovnik V, Gershman A B. A local polynomial approximation based beamforming for source localization and tracking in nonstationary environments. IEEE Signal Process Lett, 2000, 7: 3–5
26 Guo Y, Li B Z. Blind image watermarking method based on linear canonical wavelet transform and QR decomposition. IET Image Process, 2016, 10: 773–786
27 Xu T Z, Li B Z. Linear Canonical Transform and Its Application. Beijing: Science Press, 2013
28 Bu H X, Bai X, Tao R. Compressed sensing SAR imaging based on sparse representation in fractional Fourier domain. Sci China Inf Sci, 2012, 55: 1789–1800
29 Liu F, Xu H F, Tao R, et al. Research on resolution between multi-component LFM signals in the fractional Fourier domain. Sci China Inf Sci, 2012, 55: 1301–1312
30 Wei D Y, Li Y M. Generalized sampling expansions with multiple sampling rates for lowpass and bandpass signals in the fractional Fourier transform domain. IEEE Trans Signal Process, 2016, 64: 4861–4874
31 Feng Q, Li B Z. Convolution and correlation theorems for the two-dimensional linear canonical transform and its applications. IET Signal Process, 2016, 10: 125–132
32 Shi J, Liu X P, He L, et al. Sampling and reconstruction in arbitrary measurement and approximation spaces associated with linear canonical transform. IEEE Trans Signal Process, 2016, 64: 6379–6391
33 Zhang Z C. Tighter uncertainty principles for linear canonical transform in terms of matrix decomposition. Digital Signal Process, 2017, 69: 70–85
34 Wei D Y, Li Y M. The dual extensions of sampling and series expansion theorems for the linear canonical transform. Optik - Int J Light Electron Opt, 2015, 126: 5163–5167
35 Kou K I, Xu R H. Windowed linear canonical transform and its applications. Signal Process, 2012, 92: 179–188
36 Kou K I, Zhang R H, Zhang Y H. Paley-Wiener theorems and uncertainty principles for the windowed linear canonical transform. Math Method Appl Sci, 2012, 35: 2212–2132
37 Tao R, Li Y L, Wang Y. Short-time fractional Fourier transform and its applications. IEEE Trans Signal Process, 2010, 58: 2568–2580
38 Yin Q, Shen L, Lu M, et al. Selection of optimal window length using STFT for quantitative SNR analysis of LFM signal. J Syst Eng Electron, 2013, 24: 26–35
39 Varadarajan V S. Some problems involving Airy functions. Commun Stoch Anal, 2012, 1: 65–68
40 Popescu S A. Mathematical analysis II integral calculus. http://civile.utcb.ro/cmat/cursrt/ma2e.pdf